IOP Publishing Journal of Physics: Condensed Matter
J. Phys.: Condens. Matter **28** (2016) 255501 (8pp) doi:10.1088/0953-8984/28/25/255501

Electronic structure evolution of single bilayer Bi(1 1 1) film on 3D topological insulator $Bi_2Se_xTe_{3-x}$ surfaces

Tao Lei[1], Kyung-Hwan Jin[2], Nian Zhang[1], Jia-Li Zhao[1], Chen Liu[1], Wen-Jie Li[3], Jia-Ou Wang[1], Rui Wu[1], Hai-Jie Qian[1], Feng Liu[2,4,5] and Kurash Ibrahim[1,5]

[1] Insitute of High Energy of Physics, Chinese Academy of Sciences, Beijing 100049, People's Republic of China
[2] Department of Materials Science and Engineering, University of Utah, Salt Lake City, UT 84112, USA
[3] Department of Physics, Zhejiang University, Hangzhou 310027, Zhejiang, People's Republic of China
[4] Collaborative Innovation Center of Quantum, Matter, Beijing 100084, People's Republic of China

E-mail: kurash@ihep.ac.cn. and fliu@eng.utah.edu

Received 22 December 2015, revised 22 March 2016
Accepted for publication 4 April 2016
Published 10 May 2016

Abstract

The electronic state evolution of single bilayer (1BL) Bi(1 1 1) deposited on three-dimensional (3D) $Bi_2Se_xTe_{3-x}$ topological insulators at $x = 0$, 1.26, 2, 2.46, 3 is systematically investigated by angle-resolved photoemission spectroscopy (ARPES). Our results indicate that the electronic structures of epitaxial Bi films are strongly influenced by the substrate especially the topmost sublayer near the Bi films, manifesting in two main aspects. First, the Se atoms cause a stronger charge transfer effect, which induces a giant Rashba-spin splitting, while the low electronegativity of Te atoms induces a strong hybridization at the interface. Second, the lattice strain notably modifies the band dispersion of the surface bands. Furthermore, our experimental results are elucidated by first-principles band structure calculations.

Keywords: electronic structure, Bi(1 1 1) film, ARPES, interfacial interaction, topological insulator

(Some figures may appear in colour only in the online journal)

Introduction

Topological insulators (TIs)—a newly discovered quantum class of materials with topological order—have attracted intensive study in last few years [1–6]. TIs host spin-polarized surface/edge states, which are not allowed to backscatter due to constraints of time-reversal symmetry and are thus very desirable for spintronics and other applications [7–9]. The TIs show unique quantum properties that come from strong spin–orbit coupling, such as magnetic monopole [8], Majorana fermions [7], anomalous quantum Hall effect [10] and spin related novel phenomena [11]. Topologically protected by time-reversal symmetry, the one-dimensional (1D) edge states in 2D TIs (also called quantum spin Hall system) and the 2D surface states (SS) in 3D TIs are helical Dirac fermions and immune to backscattering by nonmagnetic impurities [12]. The $Bi_2(Te,Se)_3$ family members are confirmed as typical 3D TIs due to their simple single surface Dirac cone and relatively large bulk energy gap [6, 13]. Although quite a few compounds have been found to be 3D TIs [3, 4, 6, 14], up to now only HgTe/CdTe and InAs/GaSb quantum wells have been both theoretically proposed and experimentally demonstrated as 2D TI systems [1, 2], while strong evidence of topological edge states have been given for 1BL Bi(1 1 1) [15, 16].

Ultrathin Bi(1 1 1) film has recently drawn exceptional attention by the prediction that it belongs to another category of 2D TI with much shorter edge-state penetration length scale compared to that of the HgTe/CdTe quantum well

[5] Author to whom correspondence should be addressed.

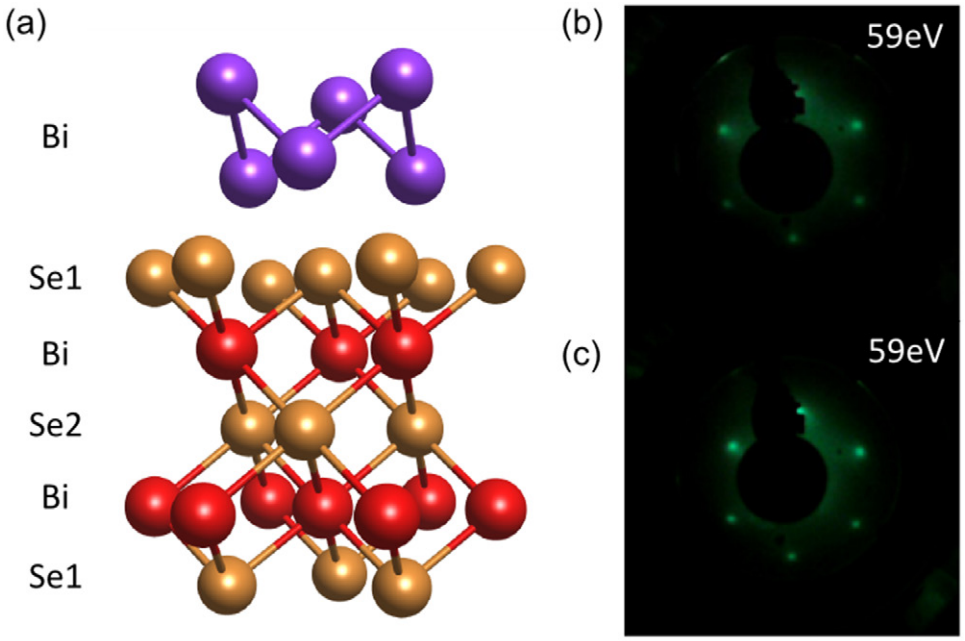

Figure 1. (a) Schematic illustration of single bilayer Bi and quintuple layer crystal structure for Bi_2Se_3. LEED patterns of the (b) 1×1 $Bi_2Se_{1.26}Te_{1.74}$ (1 1 1) and (c) 1BL Bi/$Bi_2Se_{1.26}Te_{1.74}$ at 59 eV.

[17–20]. Experimental attempts to fabricate 1BL Bi(1 1 1) on the Si(1 1 1) surface failed below 6BL thickness [21], and successful growth of the 1BL Bi(1 1 1)/Sb(1 1 1) on Bi_2Te_3(1 1 1) has been recently reported [15, 22–25]. The results show that the single BL Bi is strained assuming a pseudomorphic growth relationship to the substrate. Accordingly, the band structure is affected and Bi undergoes a topological phase transition [26]. Investigation into the influence of strain effect and interface interaction between substrates and ultrathin Bi bilayer in terms of electronic structure evolution is a direct way to inspect the nature of the two factors.

Bi_2Se_3 and Bi_2Te_3 has a layered crystal structure, made up from $Se_1(Te_1)$–Bi–$Se_2(Te_2)$–Bi–$Se_1(Te_1)$ quintuple layers (QLs) (see figure 1(a)). The QLs are perpendicular to the *c*-axis and weakly bonded together mainly by van der Waals (vdW) forces [27]. Thus the compounds are easily cleaved and the (Se_1/Te_1) sublayer is easily exposed. It has, moreover, been found by thermal and x-ray powder analysis that Bi_2Te_3 and Bi_2Se_3 form a complete solid solution in any proportion, and the solid solution ($Bi_2Se_{3-x}Te_x$) has the same crystal structure as Bi_2Te_3 [28]. With this knowledge we propose that deposition of a 1BL Bi atom on the x varied $Bi_2Se_xTe_{3-x}$ substrate surfaces should lead to modification of the surface electronic structure as a result of electronegativity and atomic radius changes by the Te/Se ratio variations [29]. To the best of our knowledge, no work on the electronic structure evolution during growth of the 1BL Bi on $Bi_2Se_xTe_{3-x}$ substrates with changing Te/Se ratio has been reported.

Experiments

Our experiments were performed in an ultra-high vacuum (UHV) system which combined a molecular beam epitaxy (MBE) growth chamber, Helium lamp ($h\nu = 21.218$ eV)-based ARPES system and synchrotron radiation Beamline 4B9B in Beijing synchrotron radiation facilities (BSRF). The base pressure of the system was better than 2×10^{-10} Torr. X-ray photoemission spectroscopy (XPS) ($h\nu = 500$ eV) was measured for every stage of the sample preparation and Au $4f_{7/2}$ photoemission was recorded for the purposes of checking the photon energies, the energy resolution was better than 0.2 eV at room temperature (RT). All the ARPES measurements were performed at 78 K, the energy and angular resolution were better than 20 meV and 0.02 $Å^{-1}$ respectively.

An n-type Si (1 1 1) wafer (P-doped, 1–10 Ω·cm at RT) was used as substrate. The Si (1 1 1) was repeatedly cleaned by resistive heating at 1523 K until a sharp 7×7 LEED pattern appeared. High purity Bi (99.999%), Se (99.999%) and Te (99.999%) were evaporated from Knudsen cells and the fluxes were calibrated by a quartz microbalance flux monitor. 10QLs films of binary Bi_2Se_3, Bi_2Te_3 and three ternary $Bi_2Se_xTe_{3-x}$ with $x = 1.26$, 2, 2.46 were grown by Bi co-evaporation either with, respectively, Se, Te or Se + Te setting the *K*-cells and substrate temperatures at adequate points [30–32]. The x values in the ternary systems are regulated through the Se evaporation time by controlling the *K*-cell shutter. LEED patterns of the 3D $Bi_2Se_{1.26}Te_{1.74}$ substrate and that of 1BL Bi/$Bi_2Se_{1.26}Te_{1.74}$ are shown in figures 1(b) and (c), respectively. The clear LEED patterns indicate the 1×1 periodicity of the $Bi_2Se_xTe_{3-x}$ (1 1 1) and 1BL Bi(1 1 1)/TI surface and also the formation of high-quality epitaxial films.

To better understand the experimental ARPES results, we also carried out first-principles DFT calculations to study the electronic structures of 1BL Bi/$Bi_2Te_xSe_{3-x}$ heterostructures as a function of x. The calculations are carried out with the Quantum Espresso package [33] using norm conserving pseudopotentials. The Perdew–Burke–Ernzerhof exchange-correlation

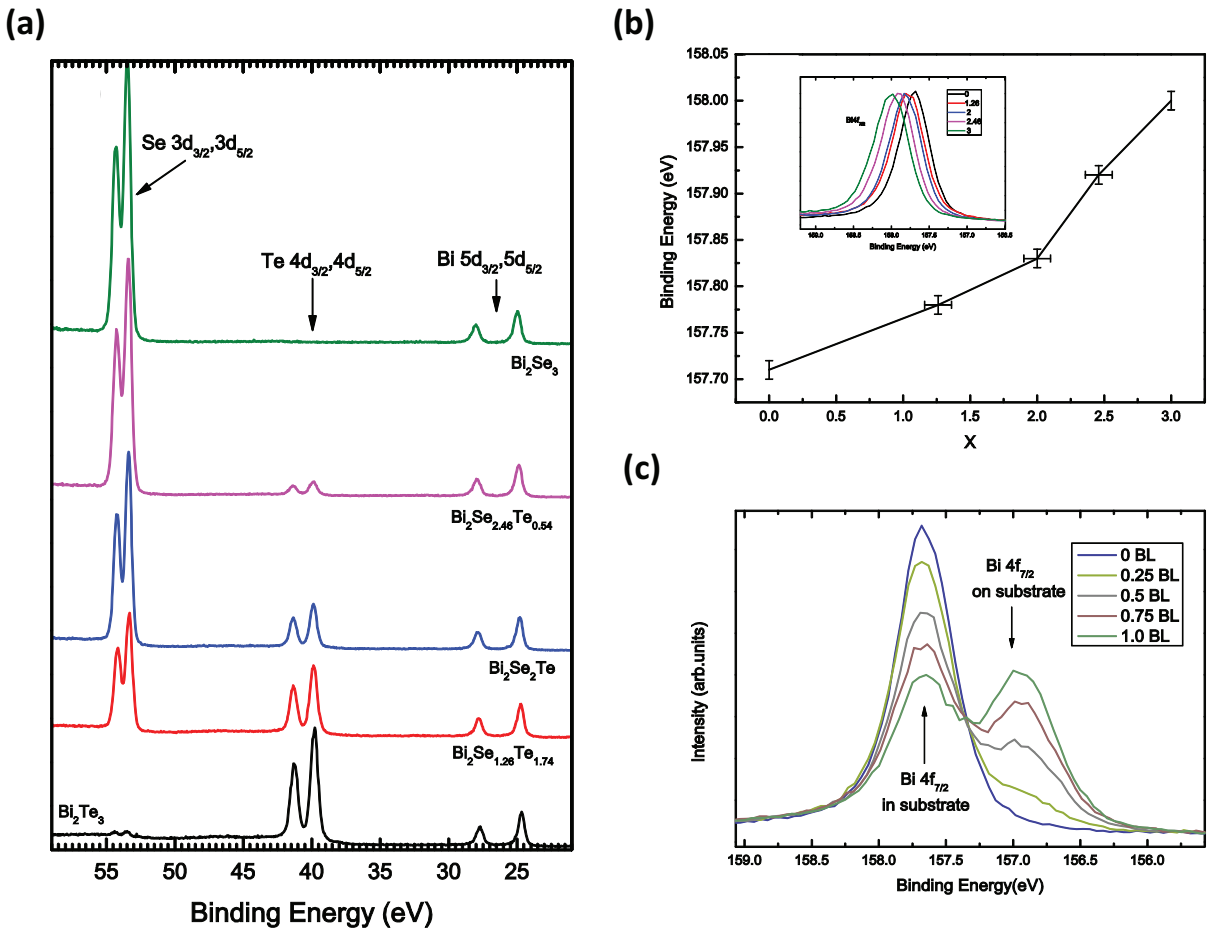

Figure 2. (a) Se 3d, Te 4d and Bi 5d core-level XPS of the $Bi_2Se_xTe_{3-x}$ samples for $x = 0$, 1.26, 2.0, 2.46 and 3.0 measured at photon energy 500 eV. (b) Bi $4f_{7/2}$ binding energy variation versus x; it shows nearly a linear relation. Inset is the Bi $4f_{7/2}$ peaks in the five samples shown in different colors. (c) The Bi $4f_{7/2}$ peak relative intensity variation of the Bi_2Te_3 substrate and that of overlayer Bi with the Bi deposition coverage. The deposition rate is carefully controlled by measuring one set of XPS every two minutes until the two peaks reached equal heights.

functional was used throughout this work. The lattice constant of the substrate are taken from experiments, and the calculations are performed with a plane-wave cutoff of 400 eV on an $11 \times 11 \times 1$ k-point mesh. The alloy substrate is modeled by a slab of 6 QL. We also employ the virtual crystal approximation (VCA) where Se and Te atoms are substituted by one effective type of atom of intermediate nuclear and electronic charge. It is generally valid when the scattering effect of disorder is weak, as may be expected here because Se and Te have the same valence electrons, same crystal structure, similar lattice constant, and do not participate in the localized states. In doing so, we effectively assumed a uniform Se and Te distribution in the $BiSe_xTe_{3-x}$ substrate. In general, the VCA approach allows calculation of disordered systems to be carried out at the same cost as calculations for ordered structures. It assumes that on each potentially disordered site there is a virtual atom which interpolates between the properties of the actual components. The VCA ignores short range order such as local distortions, but gives a good description of the overall long-range alloy properties, such as band-structures [34, 35], so it is ideally suited for our purpose here.

XPS is one of the few techniques that gives an unambiguous measure of the elemental composition at surfaces [36, 37], and one can evaluate the concentration of the atomic species in the surface layer from its peak intensity. To make sure the results are credible, wide scan spectra with binding energies ranging from 21 eV to 60 eV that include Se 3d, Te 4d and Bi 5d core-levels have been measured (see figure 2(a)). Each spectrum was normalized relative to the Bi 5d intensity, thus the relative intensity of Se 3d and Te 4d reflects the absolute variation in the atom ratios. We establish an equation to estimate the x values based on the theoretical result [36]:

$$X = (3\sigma_{Te} I_{Te} I_{Bi} - 3\sigma_{Te}^2 I_{Te}^2 + 3\sigma_{Se}^2 I_{Se}^2)/\,[I_{Bi}(\sigma_{Te} I_{Te} + \sigma_{Se} I_{Se})]$$

where I_{Te} (I_{Se}) denote the Te 4d (Se 3d) photoemission intensities, and $\sigma_{Te}(\sigma_{Se})$ is an element related factor which contains the asymmetry parameter, the total photoabsorption cross section, the density of element, etc. The value of $\sigma_{Te}(\sigma_{Se})$ can be calculated from our $Bi_2Te_3(Bi_2Se_3)$ samples: $I_{Se}\sigma_{Se} = I_{Bi}$, $I_{Te}\sigma_{Te} = I_{Bi}$. By peak fitting with the Shirley background we determine the x values (with about 10% error): $x = 0$, 1.26, 2.0, 2.46, 3.0, so the stoichiometry of the five samples is Bi_2Te_3, $Bi_2Se_{1.26}Te_{1.74}$, $Bi_2Se_2Te_1$, $Bi_2Se_{2.46}Te_{0.54}$, Bi_2Se_3.

Substitution of the less electronegativity and larger atomic radius Te by Se leads to strengthening of chemical bond with

Bi and the valence electron tends to move the Se site at some level, so the Bi 4f core-level shows a slight shift towards higher energy [38]. Figure 2(b) clearly shows such trends in five samples with the measured binding energies of the Bi to be $4f_{7/2}$ as 157.71, 157.78, 157.82, 157.92 and 158.00 eV. More importantly, the peaks in the inset in figure 2(b) appear with good uniformity without any sign of shoulder, and the FWHM of the ternary compounds $Bi_2Se_{1.26}Te_{1.74}$, $Bi_2Se_2Te_1$ and $Bi_2Se_{2.46}Te_{0.54}$ show no deviation from that of the binary compounds Bi_2Se_3 and Bi_2Te_3. This demonstrates that all the Bi atoms are in a similar chemical environment. The samples are grown phase homogeneously and the Se, Te atoms distribute uniformly.

The growth rate of the Bi bilayer has been precisely controlled through the film thickness estimation by *in situ* XPS measurement. Figure 2(c) demonstrates the Bi $4f_{7/2}$ peaks' relative intensity variations in substrate Bi and overlayer Bi along with the coverage. For the layer-by-layer growth mode, the substrate signal should be attenuated according to $I = I_0 \exp(-t/\lambda\cos\theta)$ [36]. In the 1BL $Bi/Bi_2Se_xTe_{3-x}$ systems, 1BL Bi and 1QL $Bi_2Se_xTe_{3-x}$ contain the same number of Bi atoms, then the Bi $4f_{7/2}$ in two different chemical states have the same emission intensity without considering the photoelectron attenuation. Hetero-epitaxial film in atomic-scale structure had been investigated by SXRD and LEED analysis [39, 40], and the inelastic-mean-free-path of the Bi $4f_{7/2}$ photoelectron at kinetic energy 338 eV was estimated to be ~9 Å [41]. With these initial conditions a series of photoelectron attenuation values for the two chemical environments can be estimated using the peaks' intensity and then eventually the Bi coverage can be obtained [42]. Specifically, when the two peaks have nearly equal intensity the deposited Bi reaches a single bilayer, which is also cross-checked by the quartz microbalance flux monitor.

Results and discussion

Figures 3(a), (c), (e), (g) and (i) shows the band structure of the bare $Bi_2Se_xTe_{3-x}$ ($x = 0$, 1.26, 2.0, 2.46, 3) systems near the Fermi level around the zone center ($\overline{\Gamma}$-point), the spectra are taken along the $\overline{\Gamma} - \overline{K}$ direction. Red lines mark the Dirac cone-like surface states, and blue lines the bulk valence bands (BVB). The films thickness is nearly the same (~10 QL) and this thinness guarantees the ARPES spectrum represents the intrinsic TIs for the films largely decoupled from Si (1 1 1) [43]. The states with strong intensity below the Fermi level (E_F) near the $\overline{\Gamma}$-point is of bulk conduction bands (BCB) [30]. Such phenomenon is due to the fact that the Se is a volatile element with a relatively high vapor pressure so that Se vacancy (V_{Se}) and substitutional Se_{Bi} defects are easily formed [44]. Linearly dispersive energy bands from surface states form a Dirac cone at the Γ-point which are well separated from bulk bands. Known from previous ARPES studies and first-principles calculations [6, 45], the Dirac point of Bi_2Te_3 is hidden by the 'M'-shaped BVB [46], while for Bi_2Se_3 the Dirac point is above the 'reverse U'-shaped BVB [47]. In the current systems, the Dirac point can be located at ~0.3 eV and ~0.4 eV below the Fermi level. For the ternary compounds $Bi_2Se_xTe_{3-x}$ ($x = 1.26$, 2.0, 2.46), the band dispersion of the BVB deforms from the 'M'-shape to 'reverse U'-shape gradually with the increase of x as marked with blue lines in figures 3(c), (e) and (g). DFT-calculated band structures overlaid with the experimental results show good agreement.

The electronic band structure changes dramatically when a single Bi (1 1 1) bilayer is grown on the substrates (figures 3(b), (d), (f), (h) and (j)). A pair of states marked by a_1 and a_2 (green dotted lines) show upwards dispersions from $k_{\|} \sim \pm 0.5$ Å^{-1} at ~0.6 eV below E_F and crossing at $k_{\|} \sim \pm 0.25$ Å^{-1}. This is a result of splitting of the spin-degenerate band of Bi(1 1 1) bilayer due to symmetry breaking at the interface [22]. The band a_1 crosses the Fermi surface at $k_{\|} \sim \pm 0.18$ Å^{-1}, while the a_2 turns into a wavelike band in the region from -0.2 Å^{-1} to $+0.2$ Å^{-1} below E_F. Although the band a_1 is nearly unchanged for all the systems underneath the E_F, the a_2 band shows a higher volatility with the Se content increasing and intersects with a_1 at $\overline{\Gamma}$-point (labeled by 'D_2'). At the same time, two sets of linearly dispersive bands (the upward-dispersing band marked by b and downward one by c) cross at $\overline{\Gamma}$-point (labeled as D_1 in figure 3(b)). In the Bi/Bi_2Te_3 system, the single bilayer Bi intrinsic band a_2 is strong hybridization with the Bi_2Te_3 substrate due to close energy proximity, and the crossing point for band c situates slightly at above 0.2 eV and that for b slightly below 0.2 eV, and a nondispersive feature between them with an energy width of ~50 meV was observed [23]. While in the $Bi/Bi_2Se_{1.26}Te_{1.74}$ system, the crossing moves slightly upward to 0.15 eV and the linear dispersive bands are no longer observed (figure 3(d)). For the $Bi/Bi_2Se_2Te_1$ system, band b continues to shift upward, but at the crossing point its dispersion evolves from linear to high-order bent line and crosses with c at the $\overline{\Gamma}$ point, consistent with previous calculations. This tendency is more obvious in the $Bi/Bi_2Se_{2.46}Te_{0.54}$ and Bi/Bi_2Se_3 systems, as shown in figures 3(h) and (j) [48]. It means that the Fermi group velocity of Dirac fermions near the Dirac point is changed, which originates from the hybridization between the Bi(1 1 1) BL and Dirac surface states [49]. At the same time, the spin splitting of the a_1 and a_2 band becomes more obvious, and D_1 is formed by intersection of the band b and c. The D_2 originates from the hybridization of a_2 and b bands and the two bands evolve into a giant Rashba-split state in the $Bi/Bi_2Se_{2.46}Te_{0.54}$ and Bi/Bi_2Se_3 systems [50]. These findings show that with the same single Bi bilayer on the similar and closely related $Bi_2Se_xTe_{3-x}$ substrates, the electronic structure can have a large modulation.

It is obvious that the interfacial interaction of the 1BL Bi and the substrate should be important in the very thin films [26]. Substitution of the Se for Te in $Bi_2Se_xTe_{3-x}$ is not random and the substitution process prefers first to occupy the middle layer of the quintuple. It has been shown that the Se atoms preferentially to occupy site (2) (figure 1(a)) when $x \leqslant 1$, and the excess Se distributes randomly in site (1) after site (2) is fully occupied when $x > 1$ [51]. In the latter situation, the portion of Te in the topmost layer next to the 1BL Bi counts $(3 - x)/2$, which implies that in the Bi/Bi_2Te_3 and $Bi/Bi_2Se_{1.26}Te_{1.74}$ systems the topmost layer in the substrates is almost completely composed of Te atoms. With the increasing Se content, the Te portion in the topmost layer, i.e. in site

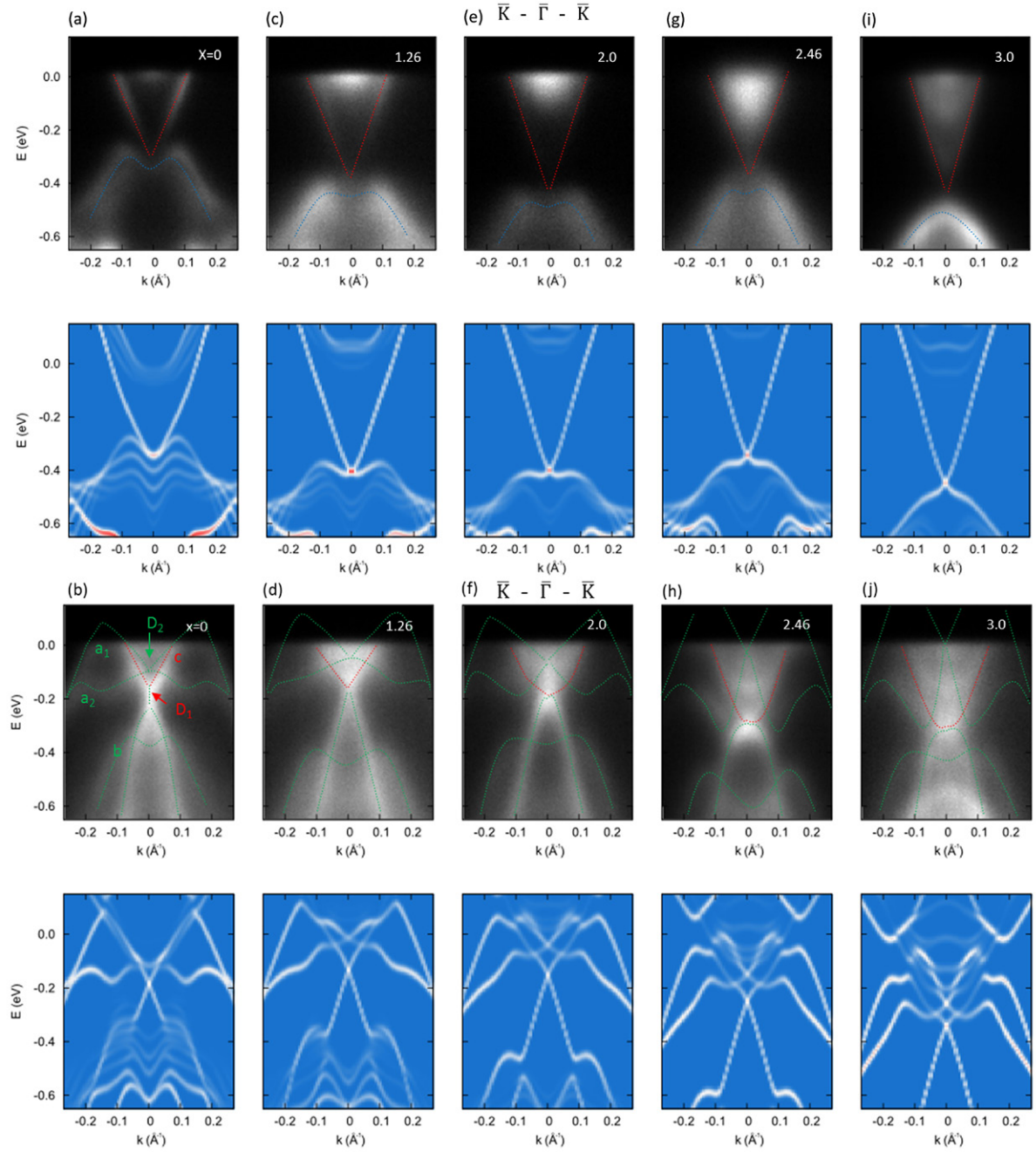

Figure 3. Experimental band dispersions along $\overline{\Gamma} - \overline{K}$ directions. (a), (c), (e), (g), (i) are the raw ARPES spectra of 10 QL $Bi_2Se_xTe_{3-x}$ TIs at $x = 0$, 1.26, 2.0, 2.46, 3.0, respectively; (b), (d), (f), (h), (j) are the ARPES for 1BL Bi grown on the $Bi_2Se_xTe_{3-x}$ substrates, correspondingly. The red dashed lines mark the surface states and blue ones the valence bands. The green dashed lines a_1, a_2 and b are the intrinsic band states of the Bi bilayer, band c is the Dirac cone of substrates. DFT calculations are overlaid with the experiment results.

(1), reduces to 50% for $x = 2.0$, 27% for $x = 2.46$ and 0 for $x = 3$. To gain deeper insight into the growth mechanism and the interaction between 1BL Bi and $Bi_2Se_xTe_{3-x}$ substrates, XPS of Bi $4f_{7/2}$ core levels was measured following deposition to determine the interfacial interaction between 1BL Bi and the $Bi_2Se_xTe_{3-x}$ substrates. As seen from figure 4(a), there are separate Bi $4f_{7/2}$ core levels for the substrate and 1 BL Bi. The fitted curves of the 1 BL Bi $4f_{7/2}$ on different substrates for $x = 0$, 1.26, 2.0, 2.46, 3 are shown in figure 4(b), and the read-off binding energy values 156.96(6), 156.97(8), 156.97(2), 157.00(4) and 157.03(1) eV. We also calculated the amount of charge transfer from the Bi atom to substrate, shown in figure 4(c).

It is generally recognized that the core-level energy shift of a central atom correlates directly with the chemical environment of immediate nearest-neighbor atoms. The Bi $4f_{7/2}$ binding energy increases from 157.71 to 158.00 eV with the substrate composition changing from Bi_2Te_3 to Bi_2Se_3, which reflects the difference in the Bi–Te and Bi–Se bonding nature. VdW interaction could also contribute to the core level shift, although its strength is weaker compared to the interatomic chemical interactions [52]. In the

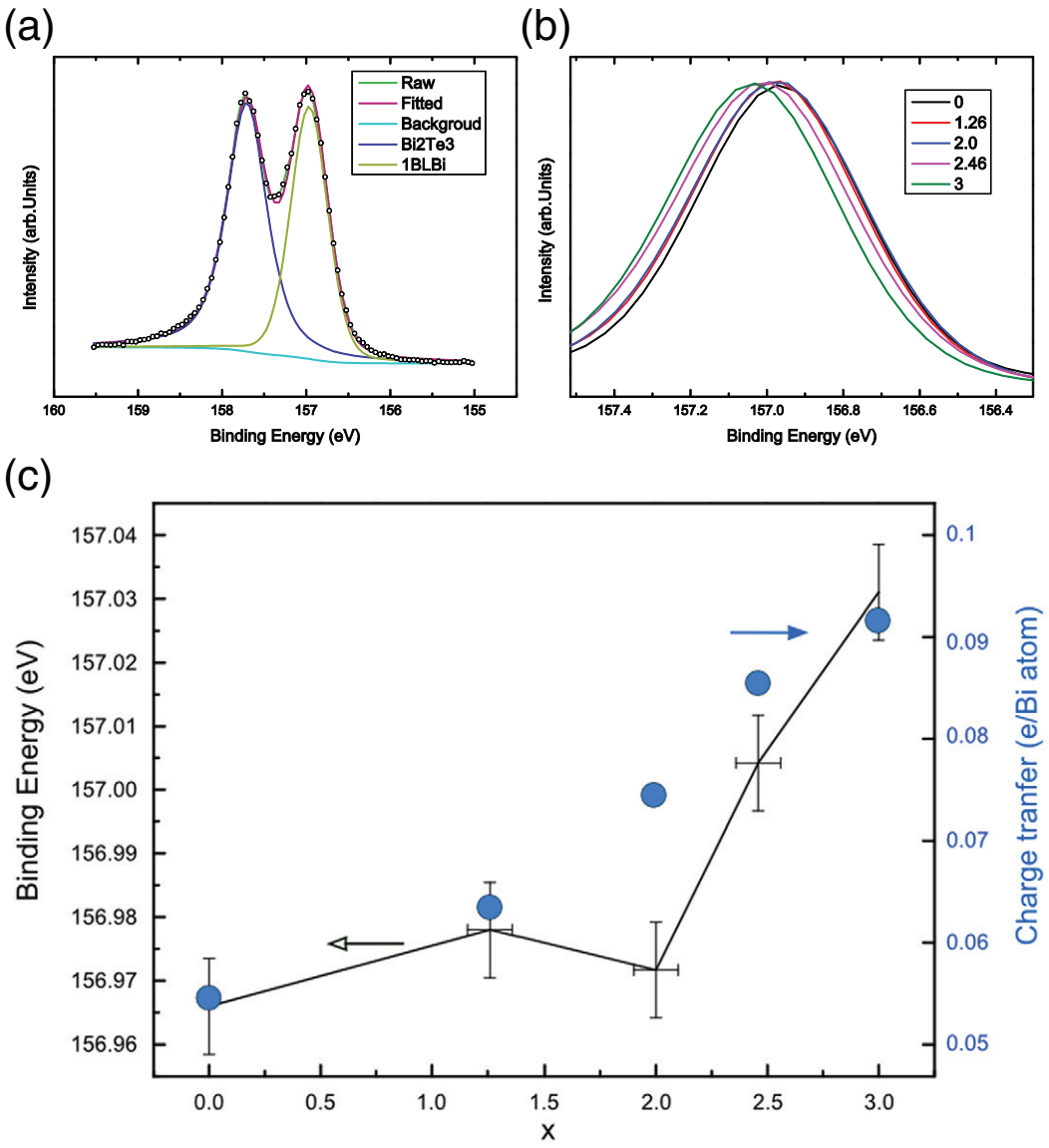

Figure 4. (a) Spectroscopic representation for the peak fitting results of the in-bilayer and in-substrate Bi $4f_{7/2}$ peaks. (b) Expanded peaks of the in-bilayer Bi $4f_{7/2}$ clearly show the peak position changes. (c) Binding energy positions of the 1BL Bi (left *Y*-axis) and the calculated charge transfer between Bi bilayer and substrates (right *Y*-axis) with increasing Se concentration.

current case, we observed the vdW force induced level shift through the 1BL Bi 4f XPS peak as seen in figure 4(c). The interaction between the bilayer and substrate in the 1BL $Bi/Bi_2Se_xTe_{3-x}$ systems should be of vdW character similar to that in the QLs. The 1BL Bi deposition on the $Bi_2Se_xTe_{3-x}$ surface reflects more or less the charge distribution in the Bi layer owing to its metallicity and higher electronegativity of the atoms in the substrate surfaces [48]. The core-level shift reflects the value of interfacial charge transfer from the Bi bilayer to substrate and the result shows the interfacial electrical field induced by charge transfer is related to the substrate. The results indicate that the interfacial electrical field stays nearly the same for the substrates with the Se atoms being distributed mostly at site (2), and it increases rapidly when distributed at site (1). The calculated charge transfer from the Bi bilayer to substrate as a function of the Se/Te ratio is show in figure 4(c). Compared with Bi/Bi_2Se_3 and Bi/Bi_2Te_3, the charge transfer at the interface in the former is much larger than that in the latter. The overall trend agrees well with the experimental results of changing Bi binding energies except for $x = 2.0$. The interfacial charge transfer affects the electronic structure of the single Bi bilayer as seen in ARPES. When the single Bi bilayer experiences a weaker electrical field ($x = 0$, 1.26 and 2), the Bi intrinsic bands a_1 and a_2 show a relatively smaller Rashba spin splitting and have strong hybridization with the substrate due to close energy proximity; such effects are also consistent with the evolution of the electronic band structure as a function of the vertical distance between the superimposed Bi bilayer and the Bi_2Se_3 slab [48]. The Rashba spin splitting increase when stronger potential gradient was introduced to the bilayer ($x = 2.46$ and 3) as see in figures 3(h) and (j), this result agrees with previous APRES data and DFT-calculated projected band structure [23, 48].

It is known that the in-plane lattice parameter a of the $Bi_2Se_xTe_{3-x}$ system decreases linearly with the increase of Se concentration, and the top 1BL Bi (1 1 1) in-plane lattice constant is compressed to match the substrates [53, 54]. The in-plane lattice constants of Bi_2Te_3 (1 1 1) and Bi_2Se_3 (1 1 1) were determined to be 4.386 Å and 4.138 Å, respectively [40, 55]. According to these parameters, the estimated corresponding lattice constants of the ternary alloys $Bi_2Se_{2.46}Te_{0.54}$, $Bi_2Se_2Te_1$, $Bi_2Se_{1.26}Te_{1.74}$ are 4.183 Å, 4.221 Å, 4.282 Å, and these in-plane parameters of Bi (1 1 1) films correspond to compressive strain values of −3.4%, −5.7%, −7.0%, −7.9% and −8.9% for $x = 0$, 1.26, 2.0, 2.46 and 3.0, respectively. First principles calculations for the single bilayer Bi show that the in-plane distortion has a great influence on the band structure [40, 56]. The original bands a_1, a_2 and b of the Bi(1 1 1) bilayer change significantly. Different from the changes induced by internal electric field in splitting the spin degeneracy of bands, the compressive strain gradually changes the band dispersion [56]. As mentioned above, the band b continues upward and gradually evolves in to ordinary Rashba-split states that hybridize with a_2, which can be attributed to the strain effects of in-plane contraction. In addition, there is a linear dispersive band of ~50 meV width in the Bi/Bi_2Te_3 system, which disappears in the system of $Bi/Bi_2Se_{1.26}Te_{1.74}$. We suggest this may be due to the upward shift of band b with the increased strain in the $Bi/Bi_2Se_{1.26}Te_{1.74}$ system that fills the band gap. This agrees with the calculated band structure results in the freestanding single bilayer Bi with varying lattice constants [40, 56].

Conclusion

In summary, we have systematically investigated a series of 1BL Bi/ $Bi_2Se_xTe_{3-x}$ hetero-epitaxial films of which the film thicknesses are precisely controlled via MBE. The linear change characters of the lattice parameters in the $Bi_2Se_xTe_{3-x}$ systems has been utilized to estimate the in-plane compressive lattice strain of the 1BL Bi film. Surface states and core-level changes are characterized by ARPES and XPS measurements. APRES results show an interesting evolution process in the surface states from Bi/Bi_2Te_3 to Bi/Bi_2Se_3, a larger Rashba splitting can be observed for the bands which are mainly contributed by the 1BL Bi(1 1 1) and hybridize with bulk states of substrate, due to the combined effects of structural relaxation and interfacial charge transfer effect. We revealed the internal electric field at the interface region combined with the effects of structural relaxation reduces the band gap and gradually induces giant Rashba splitting states. Our work significantly advances fundamental knowledge and understanding of interfacial effects in the Bi_2–$Bi_2Se_xTe_{3-x}$ systems.

Acknowledgments

This work is supported under the project 11375228 by NSFC. K-H Jin and F L acknowledge support from the US Department of Energy (Grant No. DE-FG02-04ER46148). The computations are performed on DOE-NERSC and CHPC of University of Utah.

References

[1] Bernevig B A, Hughes T L and Zhang S C 2006 Quantum spin Hall effect and topological phase transition in HgTe quantum wells *Science* **314** 1757–61
[2] Konig M, Wiedmann S, Brune C, Roth A, Buhmann H, Molenkamp L W, Qi X L and Zhang S C 2007 Quantum spin Hall insulator state in HgTe quantum wells *Science* **318** 766–70
[3] Fu L and Kane C L 2007 Topological insulators with inversion symmetry *Phys. Rev.* B **76** 045302
[4] Hsieh D, Qian D, Wray L, Xia Y, Hor Y S, Cava R J and Hasan M Z 2008 A topological Dirac insulator in a quantum spin Hall phase *Nature* **452** 970–4
[5] Hasan M Z and Kane C L 2010 Colloquium: topological insulators *Rev. Mod. Phys.* **82** 3045–67
[6] Chen Y L *et al* 2009 Experimental realization of a 3D topological insulator, Bi_2Te_3 *Science* **325** 178–81
[7] Fu L and Kane C L 2008 Superconducting proximity effect and majorana fermions at the surface of a topological insulator *Phys. Rev. Lett.* **100** 096407
[8] Qi X-L, Li R, Zang J and Zhang S-C 2009 Inducing a magnetic monopole with topological surface states *Sci. Rep.* **323** 1184
[9] Essin A M, Moore J E and Vanderbilt D 2009 Magnetoelectric polarizability and axion electrodynamics in crystalline insulators *Phys. Rev. Lett.* **102** 146805
[10] Yu R, Zhang W, Zhang H J, Zhang S C, Dai X and Fang Z 2010 Quantized anomalous Hall effect in magnetic topological insulators *Science* **329** 61–4
[11] Okada Y *et al* 2011 Direct observation of broken time-reversal symmetry on the surface of a magnetically doped topological insulator *Phys. Rev. Lett.* **106** 206805
[12] Moore J E 2010 The birth of topological insulators *Nature* **464** 194–8
[13] Xia Y *et al* 2009 Observation of a large-gap topological-insulator class with a single dirac cone Bi_2Te_3 *Nat. Phys.* **5** 398–402
[14] Hsieh D *et al* 2009 Observation of unconventional quantum spin textures in topological insulators *Science* **323** 919–22
[15] Yang F *et al* 2012 Spatial and energy distribution of topological edge states in single Bi(1 1 1) bilayer *Phys. Rev. Lett.* **109** 016801
[16] Drozdov I K, Alexandradinata A, Jeon S, Nadj-Perge S, Ji H, Cava R J, Andrei Bernevig B and Yazdani A 2014 1D topological edge states of bismuth bilayers *Nat. Phys.* **10** 664
[17] Murakami S 2006 Quantum spin hall effect and enhanced magnetic response by spin–orbit coupling *Phys. Rev. Lett.* **97** 236805
[18] Wada M, Murakami S, Freimuth F and Bihlmayer G 2011 Localized edge states in 2D topological insulators: ultrathin Bi films *Phys. Rev.* B **83** 121310
[19] Liu Z, Liu C-X, Wu Y-S, Duan W-H, Liu F and Wu J 2011 Stable nontrivial Z_{2} topology in ultrathin Bi (1 1 1) films: a first-principles study *Phy. Rev. Lett.* **107** 136805
[20] Koroteev Y M, Bihlmayer G, Chulkov E V and Blügel S 2008 First-principles investigation of structural and electronic properties of ultrathin Bi films *Phys. Rev.* B **77** 045428
[21] Nagao T, Sadowski J, Saito M, Yaginuma S, Fujikawa Y, Kogure T, Ohno T, Hasegawa Y, Hasegawa S and Sakurai T 2004 Nanofilm allotrope and phase transformation of ultrathin Bi film on Si(1 1 1)-7 × 7 *Phys. Rev. Lett.* **93** 105501
[22] Hirahara T, Bihlmayer G, Sakamoto Y, Yamada M, Miyazaki H, Kimura S I, Blugel S and Hasegawa S 2011 Interfacing 2D and 3D topological insulators: Bi(1 1 1) bilayer on Bi_2Te_3 *Phys. Rev. Lett.* **107** 166801

[23] Miao L *et al* 2013 Quasiparticle dynamics in reshaped helical Dirac *Proc. Natl Acad. Sci. USA* **110** 2758

[24] Lei T, Liu C, Zhao J-L, Li J-M, Li Y-P, Wang J-O, Wu R, Qian H-J, Wang H-Q and Ibrahim K 2016 Electronic structure of antimonene grown on Sb_2Te_3 (1 1 1) and Bi_2Te_3 substrates *J. Appl. Phys.* **119** 015302

[25] Wang Z F, Yao M Y, Ming W, Miao L, Zhu F, Liu C, Gao C L, Qian D, Jia J F and Liu F 2013 Creation of helical Dirac fermions by interfacing two gapped systems of ordinary fermions *Nat. Commun.* **4** 1384

[26] Hirahara T *et al* 2012 Atomic and electronic structure of ultrathin Bi(1 1 1) films grown on Bi_{2}Te_{3}(1 1 1) substrates: evidence for a strain-induced topological phase transition *Phys. Rev. Lett.* **109** 227401

[27] Borisova S, Krumrain J, Luysberg M, Mussler G and Grützmacher D 2012 Mode of growth of ultrathin topological insulator Bi_2Te_3 Films on Si (1 1 1) substrates *Cryst. Growth Des.* **12** 6098–103

[28] Wiese J R and Muldawer L 1960 Lattice constants of Bi_2Te_3–Bi_2Se_3 solid solution alloys *J. Phys. Chem. Solids* **15** 13–6

[29] Rowe D M 1995 *CRC Handbook of Thermoelectrics* (Boca Raton, FL: CRC Press)

[30] Li Y Y *et al* 2010 Intrinsic topological insulator Bi_2Te_3 thin films on Si and their thickness limit *Adv. Mater.* **22** 4002–7

[31] Song C L *et al* 2010 Topological insulator Bi_2Se_3 thin films grown on double-layer graphene by molecular beam epitaxy *Appl. Phys. Lett.* **97** 143118

[32] Zhang G, Qin H, Teng J, Guo J, Guo Q, Dai X, Fang Z and Wu K 2009 Quintuple-layer epitaxy of thin films of topological insulator Bi_2Se_3 *Appl. Phys. Lett.* **95** 053114

[33] Giannozzi P *et al* 2009 QUANTUM ESPRESSO: a modular and open-source software project for quantum simulations of materials *J. Phys.: Condens. Matter* **21** 395502

[34] Wang L-W, Bellaiche L, Wei S-H and Zunger A 1998 'Majjority representation' of alloy electronic states *Phys. Rev. Lett.* **80** 4725

[35] Bellaiche L and Vanderbilt D 2000 Virtual crystal approximation revisited: Application to dielectric and piezoelectric properties of perovskites *Phys. Rev.* B **61** 7877

[36] Hufner S 2003 *Photoelectron Spectroscopy Principles and Applications* (Berlin: Springer)

[37] X-ray Photoelectron Spectroscopy International (www.xpsdata.com/)

[38] Naumkin A V, Kraut-Vass A, Gaarenstroom S W and Powell C J *NIST X-Ray Photoelectron Spectroscopy Database* (U.S. Secretary of Commerce) (http://srdata.nist.gov/xps/elm_Spectra_query.aspx?Elm1=Bi&LD1=4f7%2f2&Elm2=&LD2=&Elm3=&LD3=&Elm4=&LD4=&sType=PE)

[39] Shirasawa T, Tsunoda J, Hirahara T and Takahashi T 2013 Structure of a Bi/Bi_2Te_3 heteroepitaxial film studied by x-ray crystal truncation rod scattering *Phys. Rev.* B **87** 075449

[40] Fukui N, Hirahara T, Shirasawa T, Takahashi T, Kobayashi K and Hasegawa S 2012 Surface relaxation of topological insulators: influence on the electronic structure *Phys. Rev.* B **85** 115426

[41] Free Standard Reference Databases (www.nist.gov/srd/onlinelist.cfm)

[42] Li W-j, Wang P, Wang X-X, Wang J-O, Wu R, Qian H-J, Ibrahim K, Li H-Y and Li H-N 2014 Fullerene film on metal surface: diffusion of metal atoms and interface model *Appl. Phys. Lett.* **104** 191606

[43] Liu Y, Wang H H, Bian G, Zhang Z, Lee S S, Fenter P A, Tischler J Z, Hong H and Chiang T C 2013 Interfacial bonding and structure of Bi_{2}Te_{3} topological insulator films on Si(1 1 1) determined by surface x-ray scattering *Phys. Rev. Lett.* **110** 226103

[44] Scanlon D O, King P D, Singh R P, de la Torre A, Walker S M, Balakrishnan G, Baumberger F and Catlow C R 2012 Controlling bulk conductivity in topological insulators: key role of anti-site defects *Adv. Mater.* **24** 2154–8

[45] Zhang H, Liu C-X, Qi X-L, Dai X, Fang Z and Zhang S-C 2009 Topological insulators in Bi_2Se_3, Bi_2Te_3 and Sb_2Te_3 with a single Dirac cone on the surface *Nat. Phys.* **5** 438

[46] Wang G *et al* 2011 Topological insulator thin films of Bi_2Te_3 with controlled electronic structure *Adv. Mater.* **23** 2929–32

[47] Chen Y L *et al* 2010 Massive Dirac fermion on the surface of a magnetically doped topological insulator *Science* **329** 659–62

[48] Govaerts K, Park K, De Beule C, Partoens B and Lamoen D 2014 Effect of Bi bilayers on the topological states ofBi_2Se_3: a first-principles study *Phys. Rev.* B **90** 155124

[49] Chang C-Z, Tang P, Feng X, Li K, Ma X-C, Duan W, He K and Xue Q-K 2015 Band engineering of Dirac surface states in topological-insulator-based van der Waals heterostructures *Phys. Rev. Lett.* **115** 136801

[50] Eich A, Michiardi M, Bihlmayer G, Zhu X G, Mi J L, Iversen B B, Wiesendanger R, Hofmann P, Khajetoorians A A and Wiebe J 2014 Intra- and interband electron scattering in a hybrid topological insulator: bismuth bilayer on Bi_2Se_3 *Phys. Rev.* B **90** 155414

[51] Park K, Nomura Y, Arita R, Llobet A and Louca D 2013 Local strain and anharmonicity in the bonding of $Bi_2Se_{3-x}Te_x$ topological insulators *Phys. Rev.* B **88** 224108

[52] Matena M *et al* 2010 Aggregation and contingent metal/surface reactivity of 1,3,8,10-tetraazaperopyrene (TAPP) on Cu(1 1 1) *Chemistry* **16** 2079–91

[53] Takatsuki O 1963 The crystal structure of $Bi_2Te_{3-x}Se_x$ *J. Phys. Chem. Solids* **24** 479–85

[54] He X, Zhou W, Wang Z Y, Zhang Y N, Shi J, Wu R Q and Yarmoff J A 2013 Surface termination of cleaved Bi_2Se_3 investigated by low energy ion scattering *Phys. Rev. Lett.* **110** 156101

[55] dos Reis D D *et al* 2013 Surface structure of Bi_{2}Se_{3} (1 1 1) determined by low-energy electron diffraction and surface x-ray diffraction *Phys. Rev.* B **88** 041404

[56] Chen L, Wang Z F and Liu F 2013 Robustness of 2D topological insulator states in bilayer bismuth against strain and electrical field *Phys. Rev.* B **87** 235420